Automatica 76 (2017) 345–354

Contents lists available at ScienceDirect

Automatica

journal homepage: www.elsevier.com/locate/automatica

Brief paper

Backstepping stabilization of the linearized *Saint-Venant–Exner* model☆

Ababacar Diagne [a], Mamadou Diagne [b], Shuxia Tang [c], Miroslav Krstic [c]

[a] *Division of Scientific Computing, Department of Information Technology, Uppsala University, Box 337, 75105 Uppsala, Sweden*

[b] *Department of Mechanical Engineering, University of Michigan G.G. Brown Laboratory 2350 Hayward Ann Arbor MI 48109, United States*

[c] *Department of Mechanical & Aerospace Engineering, University of California, San Diego, La Jolla, CA 92093-0411, United States*

ARTICLE INFO

Article history:
Received 3 April 2015
Received in revised form
2 September 2016
Accepted 22 September 2016
Available online 8 December 2016

Keywords:
Backstepping
State feedback controller
Output feedback controller
Saint-Venant–Exner
Hyperbolic PDEs

ABSTRACT

Using backstepping design, exponential stabilization of the linearized Saint-Venant–Exner (SVE) model of water dynamics in a sediment-filled canal with arbitrary values of canal bottom slope, friction, porosity, and water–sediment interaction, is achieved. The linearized SVE model consists of two rightward convecting transport Partial Differential Equations (PDEs) and one leftward convecting transport PDE. A single boundary input control strategy with actuation located only at the downstream gate is employed. A full state feedback controller is designed which guarantees exponential stability of the desired setpoint of the resulting closed-loop system. Using the reconstruction of the distributed state through a backstepping observer, an output feedback controller is established, resulting in the exponential stability of the closed-loop system at the desired setpoint. The proposed state and output feedback controllers can deal with both subcritical and *supercritical* flow regimes without any restrictive conditions.

© 2016 Elsevier Ltd. All rights reserved.

1. Introduction

The SVE model has attracted considerable attention over the past decades. Significant results such as Daly and Porporato (2005) and Lanzoni, Siviglia, Frascati, and Seminara (2006) are devoted to the numerical analysis of the dynamics of water flow coupled with a movable bed. However, the boundary control of such systems described by nonlinear hyperbolic PDEs is left out in most of these contributions. In the present work, we are interested in the stabilization of the SVE hyperbolic PDEs that describe the flow and the bed evolutions in an open channel (Diagne, Bastin, & Coron, 2012; Diagne & Sène, 2013). During the past decades, various control strategies, which do not account for sediment dynamics, have been developed with the aim to stabilize and to regulate water flow dynamics in irrigation channels. Usually, the openings of the gates located at the ends of the channel are controlled to achieve the stabilization of the water level and flow rate at desired setpoints. Even though controlling of the discharge remains a possible alternative, the superiority of gates openings control has been proven in many cases. We refer the reader to Malaterre, Rogers, and Schuurmans (1998), for an extensive review of control design methodologies for irrigation channels. For instance, Balogun, Hubbard, and DeVries (1988) proposed an LQ control strategy, whereas Prieur and de Halleux (2004) developed a Lyapunov-based design. Semigroup approach (Xu & Sallet, 1999), H_∞ control (Litrico & Fromion, 2006; Pognant-Gros, Fromion, & Baume, 2001) and multi-models design (Diagne, Santos Martins, & Rodrigues, 2010; Santos Martins, Rodrigues, & Diagne, 2008), to mention a few, have been exploited to regulate irrigation channel.

Based on the linearized SVE model, the control of water flow dynamics under a movable bed, is achieved by Diagne et al. (2012), employing explicit dissipative boundary conditions that ensure exponential stability in L^2-norm of one-dimensional hyperbolic systems of balance laws. Recently, boundary control of hyperbolic systems based on singular perturbation was utilized to successfully control the linearized SVE model (Tang, Prieur, & Girard, 2014). However, the two aforementioned methods require on-line measurements of the water levels at the upstream ($x = 0$) and the downstream ($x = L$) ends of the canal. Among the existing contributions, only Diagne and Sène (2013), which uses a priori estimation technique combined with Faedo–Galerkin method, enables feedback stabilization by merely sensing the downstream gate.

☆ Ababacar Diagne was supported by grants from Lisa and Carl-Gustav Esseen foundation. The material in this paper was not presented at any conference. This paper was recommended for publication in revised form by Associate Editor Tong Zhou under the direction of Editor Richard Middleton.

E-mail addresses: ababacar.diagne@it.uu.se (A. Diagne), mdiagne@umich.edu (M. Diagne), sht015@ucsd.edu (S.-X. Tang), krstic@ucsd.edu (M. Krstic).

http://dx.doi.org/10.1016/j.automatica.2016.10.017
0005-1098/© 2016 Elsevier Ltd. All rights reserved.

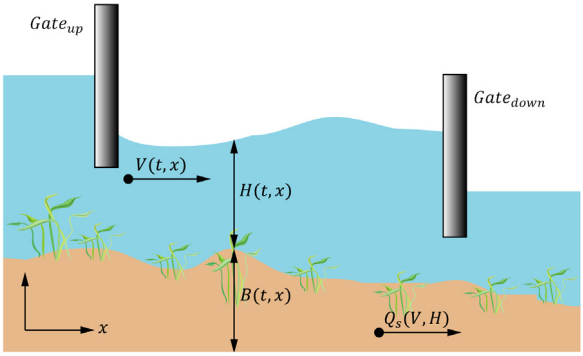

Fig. 1. A sketch of the channel.

In the recent years, PDE backstepping has proved to be of fundamental importance for boundary feedback stabilization of distributed parameter systems involving transport and diffusion phenomena (Coron, Vazquez, Krstic, & Bastin, 2013; Di Meglio, Vazquez, & Krstic, 2013; Krstic & Smyshlyaev, 2008). The key point of backstepping is the construction of a suitable Volterra integral transformation that maps an original PDE system into a so-called "target system" whose exponential stability is easier to establish. Based on the invertibility of the transformation, the original and the target system have equivalent stability. The kernel functions of such a transformation are required to satisfy some PDEs whose solutions are used as gains of the original system controller.

In the present work, we achieve exponential stabilization of the linearized Saint-Venant–Exner (SVE) model that describes water dynamics in a sediment-filled canal with arbitrary values of bottom slope, friction, porosity, and water–sediment interaction (Diagne et al., 2012). The backstepping design (Di Meglio et al., 2013) is employed to construct the boundary feedback control action for the stabilization of two rightward and one leftward convecting PDEs derived from the linearization of the SVE model. The proposed controller enables the stabilization of both subcritical and supercritical flow regimes, which has not been the case in previous results (Diagne et al., 2012; Diagne & Sène, 2013). By solely considering an actuation of the downstream gate, a full state feedback controller is designed to ensure the exponential stabilization of the closed-loop system at the desired setpoint. Designing an exponentially convergent Luenberger observer that enables the reconstruction of the distributed state, an output feedback controller is built using only available measurements at the upstream gate. The properties of the flow depend on the dimensionless Froude number (Fr). The proposed controllers operate under both subcritical ($Fr < 1$) and supercritical ($Fr > 1$) flow regimes. Particularly, the stabilization of a supercritical flow regime for which the water flow involves a high velocity and a low height setpoint values, is extremely hard to achieve. Moreover, exponential stability results are achieved without the need to impose restrictive conditions on the matrix arising from the source term of the system. Conversely, that matrix is required to satisfy a restrictive condition to be marginally diagonally stable (Diagne et al., 2012).

This paper is organized as follows. In the next section, the nonlinear SVE model is described. Section 3 introduces the backstepping transformation which converts the linearized SVE model into an exponentially stable target system, and the full state feedback controller is designed. An exponentially convergent backstepping observer is designed in Section 4. Based on the observer, which reconstructs the full state from the output measurement, an output feedback controller is constructed in Section 5, and exponential stability at the equilibrium setpoint of the resulting closed-loop system is also established. Numerical simulations are provided for the supercritical flow regime in Section 6. The paper ends with concluding remarks and future directions stated in Section 7.

2. The Saint-Venant–Exner model

We consider a pool of a prismatic sloping open channel with a rectangular cross-section, a unit width, and a moving bathymetry. The water depth $H(t,x)$, the water velocity $V(t,x)$ and the bathymetry $B(t,x)$ which is the depth of the sediment layer above the channel bottom, are defined as the state variables of the model (see Fig. 1). The dynamics of the system are described by the coupling of Saint-Venant and Exner equations (see e.g. Hudson & Sweby, 2003)

$$\frac{\partial H}{\partial t} + V\frac{\partial H}{\partial x} + H\frac{\partial V}{\partial x} = 0, \tag{1a}$$

$$\frac{\partial V}{\partial t} + V\frac{\partial V}{\partial x} + g\frac{\partial H}{\partial x} + g\frac{\partial B}{\partial x} = gS_b - C_f\frac{V^2}{H}, \tag{1b}$$

$$\frac{\partial B}{\partial t} + aV^2\frac{\partial V}{\partial x} = 0, \tag{1c}$$

where, g is the gravity constant, S_b is the bottom slope of the channel, C_f is a friction coefficient and a is a parameter that encompasses the porosity and viscosity effects on the sediment dynamics. The coefficient a expresses as (cf. Hudson & Sweby, 2003) $a = \frac{3A_g}{1-p_g}$, with p_g being the porosity parameter and A_g is the coefficient to control the interaction between the bed and the water flow.

2.1. The Linearized model of SVE and its representation in Riemann coordinates

In order to linearize the model (1) around a steady-state, we introduce the following vector

$$\begin{pmatrix} h & u & b \end{pmatrix}^{tr} = \begin{pmatrix} H - H^* & V - V^* & B - B^* \end{pmatrix}^{tr}.$$

Here, a steady-state is a constant state $(H^*, V^*, B^*)^T$ which satisfies the relation $gS_bH^* = C_fV^{*2}$ and the linearized model of (1) is written as follows

$$\frac{\partial W}{\partial t} + \boldsymbol{A}(W^*)\frac{\partial W}{\partial x} = \boldsymbol{B}(W^*)W, \tag{2}$$

where $W = \begin{pmatrix} h & u & b \end{pmatrix}^{tr}$,

$$\boldsymbol{A}(W^*) = \begin{pmatrix} V^* & H^* & 0 \\ g & V^* & g \\ 0 & aV^{*2} & 0 \end{pmatrix},$$

$$\boldsymbol{B}(W^*) = \begin{pmatrix} 0 & 0 & 0 \\ C_f\frac{V^{*2}}{H^{*2}} & -2C_f\frac{V^*}{H^*} & 0 \\ 0 & 0 & 0 \end{pmatrix}.$$

Exact, but rather complicated expressions of the eigenvalues λ_i of $\boldsymbol{A}(W^*)$ can be obtained by using the *Cardano-Vieta* method, see Hudson and Sweby (2003). For the sake of simplicity, we introduce the notation $r_k = C_f\frac{V^*}{H^*}\frac{\lambda_k}{(\lambda_k-\lambda_i)(\lambda_k-\lambda_j)}$. After some computations, (2) can be written as:

$$\frac{\partial \xi_k}{\partial t} + \lambda_k\frac{\partial \xi_k}{\partial x} + \sum_{s=1}^{3}(2\lambda_s - 3V^*)r_s\xi_s = 0, \quad k = 1, 2, 3, \tag{3}$$

where the characteristic coordinates are

$$\xi_k = \frac{H^*}{C_fV^*\lambda_k}\Big[\big((V^* - \lambda_i)(V^* - \lambda_j) + gH^*\big)h + H^*\lambda_k u + gH^*b\Big]. \tag{4}$$

Using (3), we rewrite (2) in characteristic form as

$$\frac{\partial \boldsymbol{\xi}}{\partial t} + \boldsymbol{\Lambda}\frac{\partial \boldsymbol{\xi}}{\partial x} - \boldsymbol{M}\boldsymbol{\xi} = 0, \tag{5}$$

$$\boldsymbol{\xi} = (\xi_1, \xi_2, \xi_3)^T, \qquad \boldsymbol{\Lambda} = diag(\lambda_1, \lambda_2, \lambda_3), \tag{6}$$

$$\boldsymbol{M} = \begin{pmatrix} \alpha_1 & \alpha_2 & \alpha_3 \\ \alpha_1 & \alpha_2 & \alpha_3 \\ \alpha_1 & \alpha_2 & \alpha_3 \end{pmatrix}, \qquad \alpha_k = \left(3V^* - 2\lambda_k\right) r_k. \tag{7}$$

2.2. Control problem statement

From the representation of the linearized SVE model in Riemann coordinates defined in (7), we derive a boundary control problem which is similar to the control problem solved (Di Meglio et al., 2013). First, we redefine the state variables as

$$v(t,x) = \xi_1(t,x), \qquad u_1(t,x) = \xi_2(t,x), \qquad u_2(t,x) = \xi_3(t,x)$$

and, the characteristics velocities as

$$\lambda_1 = -\mu, \qquad \gamma_1 = \lambda_2, \qquad \gamma_2 = \lambda_3.$$

Next, we adopt the following notations for the coefficients of the matrix $\boldsymbol{M}$ defined in (7)

$$\eta_j = \alpha_{j+1}, \quad \text{for } j = \{1,\ 2\}, \qquad \boldsymbol{\sigma} = \begin{pmatrix} \alpha_2 & \alpha_3 \\ \alpha_2 & \alpha_3 \end{pmatrix}.$$

Hence, the system (5)–(7) is rewritten as follow

$$\partial_t u_1 + \gamma_1 \partial_x u_1 = \sigma_{11} u_1 + \sigma_{12} u_2 + \alpha_1 v, \tag{8a}$$

$$\partial_t u_2 + \gamma_2 \partial_x u_2 = \sigma_{21} u_1 + \sigma_{22} u_2 + \alpha_1 v, \tag{8b}$$

$$\partial_t v - \mu \partial_x v = \eta_1 u_1 + \eta_2 u_2 + \alpha_1 v. \tag{8c}$$

The change of variable $w(t,x) = v(t,x)\exp\left(-\frac{\alpha_1}{\mu}x\right)$ transforms system (8) into the following form

$$\partial_t u_1 + \gamma_1 \partial_x u_1 = \sigma_{11} u_1 + \sigma_{12} u_2 + \alpha(x) w, \tag{9a}$$

$$\partial_t u_2 + \gamma_2 \partial_x u_2 = \sigma_{21} u_1 + \sigma_{22} u_2 + \alpha(x) w, \tag{9b}$$

$$\partial_t w - \mu \partial_x w = \theta_1(x) u_1 + \theta_2(x) u_2, \tag{9c}$$

$$u_i(t,0) = q_i w(t,0) \quad \text{for } i = 1,\ 2, \tag{9d}$$

$$w(t,1) = \rho_1 u_1(t,1) + \rho_2 u_2(t,1) + U(t), \tag{9e}$$

$$w(0,x) = w^0(x), \qquad u_i(0,x) = u_i^0(x) \quad \text{for } i = 1,\ 2 \tag{9f}$$

with $\alpha(x) = \alpha_1 \exp\left(\frac{\alpha_1}{\mu}x\right)$, $\theta_j(x) = \alpha_{j+1}\exp\left(\frac{\alpha_1}{\mu}x\right)$, $j = 1,\ 2$.

Remark 1. From the physical model (1), (2), the dimensionless Froude number is defined as $Fr = \frac{V^*}{\sqrt{gH^*}}$. For a subcritical flow regime ($Fr < 1$), the three eigenvalues of the matrix $\boldsymbol{A}$ satisfy $\lambda_1 < 0 < \lambda_2 \ll \lambda_3$ whereas, $\lambda_2 < 0 < \lambda_1 < \lambda_3$ for the supercritical one ($Fr > 1$) (Hudson & Sweby, 2003). Here, λ_1 and λ_3 are the characteristic velocities of the water flow and λ_2 is the characteristic velocity of the sediment motion. When the flow regime is supercritical, the following changes of variable $v(t,x) = \xi_2(t,x)$, $u_1(t,x) = \xi_1(t,x)$, $u_2(t,x) = \xi_3(t,x)$ and coefficients $\lambda_2 = -\mu$, $\gamma_1 = \lambda_1$ and $\gamma_2 = \lambda_3$ need to be considered.

3. Full state controller design

3.1. Backstepping transformation and target system

Consider the following backstepping transformation (Di Meglio et al., 2013)

$$\psi_i(t,x) = u_i(t,x) \quad \text{for } i = 1,\ 2 \tag{10}$$

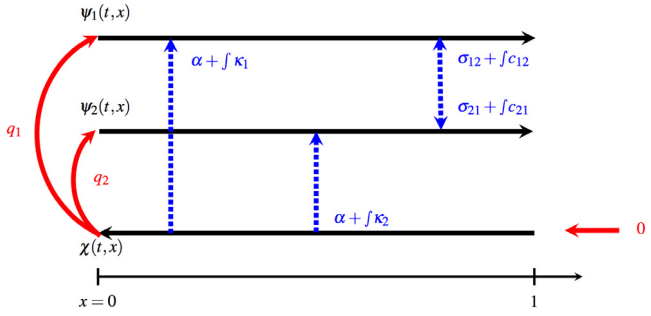

Fig. 2. Representation of the target system.

$$\chi(t,x) = w(t,x) - \int_0^x k_1(x,\xi) u_1(t,\xi)\, d\xi - \int_0^x k_2(x,\xi) u_2(t,\xi)\, d\xi - \int_0^x k_3(x,\xi) w(t,\xi)\, d\xi. \tag{11}$$

We would like the transformation (10)–(11) to map (9) into the following target system (see Fig. 2)

$$\partial_t \psi_1 + \gamma_1 \partial_x \psi_1 = \sigma_{11}\psi_1 + \sigma_{12}\psi_2 + \alpha(x)\chi + \int_0^x c_{11}(x,\xi)\psi_1(t,\xi)\, d\xi + \int_0^x c_{12}(x,\xi)\psi_2(t,\xi)\, d\xi + \int_0^x \kappa_1(x,\xi)\chi(t,\xi)\, d\xi, \tag{12a}$$

$$\partial_t \psi_2 + \gamma_2 \partial_x \psi_2 = \sigma_{21}\psi_1 + \sigma_{22}\psi_2 + \alpha(x)\chi + \int_0^x c_{21}(x,\xi)\psi_1(t,\xi)\, d\xi + \int_0^x c_{22}(x,\xi)\psi_2(t,\xi)\, d\xi + \int_0^x \kappa_2(x,\xi)\chi(t,\xi)\, d\xi, \tag{12b}$$

$$\partial_t \chi - \mu \partial_x \chi = 0, \tag{12c}$$

$$\psi_i(t,0) = q_i \chi(t,0) \quad \text{for } i = 1,\ 2 \text{ and } \chi(t,1) = 0, \tag{12d}$$

where $c_{ij}(\cdot)$ and $\kappa_i(\cdot)$ are functions to be determined on the triangular domain $\mathbb{T} = \left\{(x,\xi) \in \mathbb{R}^2 |\ 0 \le \xi \le x \le 1\right\}$. A sufficient condition for the transformation (10)–(11) to map (9) into (12) is that the kernels k_i satisfy the following PDEs

$$\mu\partial_x k_1(x,\xi) - \gamma_1 \partial_\xi k_1(x,\xi) = \sigma_{11}k_1(x,\xi) + \sigma_{21}k_2(x,\xi) + \theta_1(\xi)k_3(x,\xi), \tag{13a}$$

$$\mu\partial_x k_2(x,\xi) - \gamma_2 \partial_\xi k_2(x,\xi) = \sigma_{12}k_1(x,\xi) + \sigma_{22}k_2(x,\xi) + \theta_2(\xi)k_3(x,\xi), \tag{13b}$$

$$\mu\partial_x k_3(x,\xi) + \mu\partial_\xi k_3(x,\xi) = \alpha(\xi)k_1(x,\xi) + \alpha(\xi)k_2(x,\xi), \tag{13c}$$

$$k_1(x,x) = -\frac{\theta_1(x)}{\gamma_1 + \mu}, \qquad k_2(x,x) = -\frac{\theta_2(x)}{\gamma_2 + \mu}, \tag{13d}$$

$$\mu k_3(x,0) = q_1\gamma_1 k_1(x,0) + q_2\gamma_2 k_2(x,0). \tag{13e}$$

The existence, uniqueness and continuity of the solutions to the system (13) are established in Di Meglio et al. (2013). Substituting (10)–(11) into (12) and using (9), we deduce the following equality

$$\int_0^x \Big[\alpha(\xi)k_1(x,\xi) - c_{i1}(x,\xi) + \int_\xi^x \kappa_1(x,s)k_1(s,\xi)\, ds\Big] u_1(\xi)\, d\xi + \int_0^x \Big[\alpha(\xi)k_2(x,\xi) - c_{i2}(x,\xi)$$

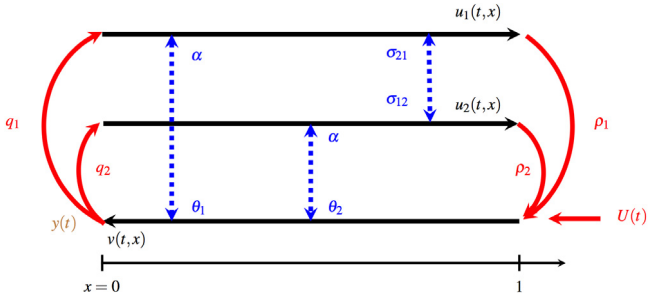

Fig. 3. Schematic steep of the hyperbolic system.[1]

$$+\int_\xi^x \kappa_2(x,s)k_2(s,\xi)\,ds\Big]u_2(\xi)\,d\xi + \int_0^x\Big[\alpha(\xi)k_3(x,\xi) - \kappa_i(x,\xi) + \int_\xi^x \kappa_1(x,s)k_3(s,\xi)\,ds + \kappa_2(x,s)k_3(s,\xi)\,ds,\Big]w(\xi)\,d\xi = 0 \tag{14}$$

where κ_i and c_{ij} satisfy the following integral equations

$$\kappa_i(x,\xi) = \alpha(x)k_3(x,\xi) + \int_\xi^x \kappa_i(x,s)k_3(s,\xi)\,ds, \quad i=\{1,\ 2\}$$
$$c_{ij}(x,\xi) = \alpha(x)k_j(x,\xi) + \int_\xi^x \kappa_i(x,s)k_j(s,\xi)\,ds, \quad i,\ j=\{1,\ 2\}.$$

3.2. Inverse transformation and control law

To ensure that the target system and the closed-loop system have equivalent stability properties, the transformation (10)–(11) has to be invertible. Since $\psi_i = u_i$, for $i = 1,\ 2$, the transformation (11) can be rewritten as

$$\chi(t,x) + \int_0^x k_1(x,\xi)\psi_1(t,\xi)\,d\xi + \int_0^x k_2(x,\xi)\psi_2(t,\xi)\,d\xi = w(t,x) - \int_0^x k_3(x,\xi)w(t,\xi)\,d\xi.$$

Let us define

$$\Gamma(t,x) = \chi(t,x) + \int_0^x k_1(x,\xi)\psi_1(t,\xi)\,d\xi + \int_0^x k_2(x,\xi)\psi_2(t,\xi)\,d\xi. \tag{15}$$

Knowing that k_3 is continuous (see. Theorem 5.3 in Di Meglio et al., 2013), there exists a unique continuous inverse kernel l_3 defined on $\mathbb{T}$, such that

$$w(t,x) = \Gamma(t,x) + \int_0^x l_3(x,\xi)\Gamma(t,\xi)\,d\xi. \tag{16}$$

Hence, from (9) and (12) we get

$$\alpha(x)w = \alpha(x)\chi + \int_0^x c_{11}(x,\xi)\psi_1(t,\xi)\,d\xi + \int_0^x c_{12}(x,\xi)\psi_2(t,\xi)\,d\xi + \int_0^x \kappa_1(x,\xi)\chi(t,\xi)\,d\xi. \tag{17}$$

[1] Figs. 2 and 3 are depicted in Di Meglio et al. (2013) for the general $n+1$ system. Fig. 3 describes the interconnection among the states, the input and the measured output of system (9).

It follows that

$$w(t,x) = \chi(t,x) + \int_0^x l_1(x,\xi)\psi_1(t,\xi)\,d\xi + \int_0^x l_2(x,\xi)\psi_2(t,\xi)\,d\xi + \int_0^x l_3(x,\xi)\chi(t,\xi)\,d\xi, \tag{18}$$

where

$$l_i(x,\xi) = k_i(t,\xi) + \int_\xi^x k_i(x,\xi)l_3(\xi,s)\,ds, \quad i=\{1,\ 2\}. \tag{19}$$

The control law $U(t)$ is obtained by substituting the transformation (11) into (9). Readily, $\chi(t,1) = 0$ implies that

$$U(t) = -\rho_1 u_1(t,1) - \rho_2 u_2(t,1) + \int_0^1\Big[k_1(1,\xi)u_1(x,\xi) + k_2(1,\xi)u_2(x,\xi) + k_3(1,\xi)w(1,\xi)\Big]d\xi, \tag{20}$$

where the gain functions k_1, k_2 and k_3 satisfy (13).

3.3. Stability of the closed-loop system

In order to establish the stability of the closed-loop system to the desired equilibrium, we first prove the exponential stability of the target system based on Lyapunov argument.

Lemma 1. *For any given initial condition* $(\psi_1^0,\ \psi_2^0,\ \chi^0)^T \in \left(\mathscr{L}^2([0,1])\right)^3$ *and under the assumption that* $c_{ij},\ \kappa_i \in \mathscr{C}(\mathbb{T})$, *the equilibrium* $(\psi_1,\ \psi_2,\ \chi)^T = (0,\ 0,\ 0)^T$ *of the target system (12a)–(12d) is* $\mathscr{L}^2$*-exponentially stable.*

Proof. Consider the following Lyapunov function

$$V_1(t) = \int_0^1\Big[a_1 e^{-\delta_1 x}\left(\frac{\psi_1^2(t,x)}{\gamma_1} + \frac{\psi_2^2(t,x)}{\gamma_2}\right) + \frac{1+x}{\mu}\chi^2(t,x)\Big]dx, \tag{21}$$

where a_1 and δ_1 are positive parameters to be determined. Differentiating (21) with respect to time along the solutions of the target system (12) and integrating by parts we get

$$\begin{aligned}\dot V_1(t) = &\Big[-a_1 e^{-\delta_1 x}(\psi_1^2(t,x) + \psi_2^2(t,x)) + (1+x)\chi^2(t,x)\Big]_0^1 \\ &- \int_0^1 \chi^2(t,x)\,dx + \int_0^1 a_1 e^{-\delta_1 x} \\ &\times\ \Psi^T(t,x)\left(-\delta_1 I_2 + 2\boldsymbol{\Gamma}_{inv}\boldsymbol{\sigma}\right)\Psi(t,x)\,dx \\ &+ 2\int_0^1 a_1 e^{-\delta_1 x}\Psi^T(t,x)\boldsymbol{\Gamma}_{inv}\boldsymbol{\alpha}(x)\chi(t,x)\,dx \\ &+ 2\int_0^1 a_1 e^{-\delta_1 x}\int_0^x \Psi^T(t,x)\boldsymbol{\Gamma}_{inv} \\ &\times\ (\boldsymbol{C}(x,\xi)\Psi(t,\xi) + K(x,\xi)\chi(t,\xi))\,d\xi\,dx,\end{aligned} \tag{22}$$

where the vectors $\Psi(t,x)$, $\boldsymbol{\alpha}(x)$, $K(x,\xi)$ and the matrices $\boldsymbol{\Gamma}_{inv}$, $\boldsymbol{C}(x,\xi)$ are given by $\Psi(t,x) = \begin{pmatrix}\psi_1(t,x)\\ \psi_2(t,x)\end{pmatrix}$, $\boldsymbol{\alpha}(x) = \begin{pmatrix}\alpha(x)\\ \alpha(x)\end{pmatrix}$, $K(x,\xi) = \begin{pmatrix}\kappa_1(x,\xi)\\ \kappa_2(x,\xi)\end{pmatrix}$, $\boldsymbol{\Gamma}_{inv} = \begin{pmatrix}\frac{1}{\gamma_1} & 0\\ 0 & \frac{1}{\gamma_2}\end{pmatrix}$, $\boldsymbol{C}(x,\xi) = \begin{pmatrix}c_{11}(x,\xi) & c_{12}(x,\xi)\\ c_{21}(x,\xi) & c_{22}(x,\xi)\end{pmatrix}$. Assume that for $M > 0$ and $\varepsilon > 0$, we have $\|\boldsymbol{\sigma}\|$, $\|\boldsymbol{\alpha}(x)\|$, $\|\boldsymbol{C}(x,\xi)\|$, $\|K(x,\xi)\| \le M$, and $\gamma_i(x) > \varepsilon, \forall i = 1,2, \forall x \in [0,1], \xi \in [0,x]$, where the matrix/vector norms $\|\cdot\|$ are compatible with the other corresponding matrix/vector norms.

Hence, using Young's inequalities, we derive the following bounds for the integral terms in (22)

$$2\int_0^1 a_1 e^{-\delta_1 x}\Psi^T(t,x)\boldsymbol{\Gamma}_{inv}\boldsymbol{\sigma}\Psi(t,x)\,dx \le 2\frac{M}{\varepsilon}\int_0^1 a_1 e^{-\delta_1 x}\Psi^T(t,x)\Psi(t,x)\,dx, \tag{23}$$

$$2\int_0^1 a_1 e^{-\delta_1 x}\Psi^T(t,x)\boldsymbol{\Gamma}_{inv}\boldsymbol{\alpha}(x)\chi(t,x)\,dx \le a_1\left(\frac{M}{\varepsilon}\right)^2\int_0^1 e^{-\delta_1 x}\Psi^T(t,x)\Psi(t,x)dx + a_1\int_0^1 e^{-\delta_1 x}\chi^2(t,x)dx, \tag{24}$$

$$2\int_0^1 a_1 e^{-\delta_1 x}\int_0^x \Psi^T(t,x)\boldsymbol{\Gamma}_{inv}\boldsymbol{C}(x,\xi)\Psi(t,\xi)\,d\xi\,dx \le a_1\int_0^1 e^{-\delta_1 x}\left(\frac{M}{\varepsilon}x+\frac{M}{\delta_1\varepsilon}\right)\Psi^T(t,x)\Psi(t,x)dx, \tag{25}$$

and

$$2\int_0^1 a_1 e^{-\delta_1 x}\int_0^x \Psi^T(t,x)\boldsymbol{\Gamma}_{inv}K(x,\xi)\chi(t,\xi)\,d\xi\,dx \le a_1\left(\frac{M}{\varepsilon}\right)^2\int_0^1 e^{-\delta_1 x}x\Psi^T(t,x)\Psi(t,x)dx + a_1\frac{1}{\delta_1}\int_0^1 e^{-\delta_1 x}\chi^2(t,x)dx. \tag{26}$$

Using the boundary conditions (23)–(26) and (12d) in (22), we derive the following estimate:

$$\dot V_1(t) \le \left(a_1\sum_{i=1}^2 q_i^2 - 1\right)\chi^2(t,0) - \int_0^1\left(1-a_1\left(1+\frac{1}{\delta_1}\right)e^{-\delta_1 x}\right)\chi^2(t,x)\,dx - a_1\int_0^1 e^{-\delta_1 x}\Psi^T(t,x)P(x)\Psi(t,x)\,dx, \tag{27}$$

$$P(x) = \left(\delta_1 - 2\frac{M}{\varepsilon} - \frac{M}{\varepsilon}x - 2\left(\frac{M}{\varepsilon}\right)^2 - \frac{M}{\delta_1\varepsilon}\right)I_2 - 2\boldsymbol{\Gamma}_{inv}\boldsymbol{\sigma}.$$

First, we choose the tuning parameter $\delta_1 > 0$ sufficiently large so that the matrix $P(x)$, $x \in [0,1]$ is positive definite. Then, by choosing

$$0 < a_1 < \min\left\{1\Big/\left(\sum_{i=1}^2 q_i^2\right), \frac{\delta_1}{\delta_1+1}\right\}, \tag{28}$$

we derive exponential stability of the target system. Then, from the continuity and invertibility of the backstepping transformation (10)–(11), we derive equivalence between the original system (9) (with the control law (20)) and the target system (12). Thus, the following theorem holds.

Theorem 1. *Consider the system (9) and the control law (20). Then under the assumptions that the initial data are in $\left(\mathscr{L}^2([0,1])\right)^3$, the origin is exponentially stable in the $\mathscr{L}^2$ sense.*

4. Backstepping observer design

The feedback controller (20) requires a full state measurement across the spatial domain. In this section, we are interested in the design of a boundary state observer for estimation of the distributed states of the system (9) over the whole spatial domain using the measured output $w(t,0) = y(t)$. We introduce the observer (Di Meglio et al., 2013)

$$\partial_t\hat u_1 + \gamma_1\partial_x\hat u_1 = \sigma_{11}\hat u_1 + \sigma_{12}\hat u_2 + \alpha(x)\hat w - p_1(x)[y(t)-\hat w(t,0)], \tag{29a}$$

$$\partial_t\hat u_2 + \gamma_2\partial_x\hat u_2 = \sigma_{21}\hat u_1 + \sigma_{22}\hat u_2 + \alpha(x)\hat w - p_2(x)[y(t)-\hat w(t,0)], \tag{29b}$$

$$\partial_t\hat w - \mu\partial_x\hat w = \theta_1(x)\hat u_1 + \theta_2(x)\hat u_2 - p_3(x)[y(t)-\hat w(t,0)], \tag{29c}$$

$$\hat u_i(t,0) = q_i y(t) \quad \text{for } i=1,2 \tag{29d}$$

$$\hat w(t,1) = \rho_1\hat u_1(t,1) + \rho_2\hat u_2(t,1) + U(t), \tag{29e}$$

where $(\hat u_1,\ \hat u_2,\ \hat w)^T$ is the estimated state vector. The functions $\theta_j(x) = \alpha_{j+1}$ for $j = 1, 2$ and $\alpha(x)$ are the ones defined for the transformed system (9).

Our objective is to find $p_1(x)$, $p_2(x)$ and $p_3(x)$ such that $(\hat w,\ \hat u_1,\ \hat u_2)$ converges to $(w,\ u_1,\ u_2)$ in finite time. Defining

$$\begin{pmatrix}\tilde w & \tilde u_1 & \tilde u_2\end{pmatrix}^T = \begin{pmatrix}w-\hat w & u_1-\hat u_1 & u_2-\hat u_2\end{pmatrix}^T \tag{30}$$

leads to the following error system

$$\partial_t\tilde w - \mu\partial_x\tilde w = \theta_1(x)\tilde u_1 + \theta_2(x)\tilde u_2 + p_3(x)\tilde w(t,0) \tag{31a}$$

$$\partial_t\tilde u_1 + \gamma_1\partial_x\tilde u_1 = \sigma_{11}\tilde u_1 + \sigma_{12}\tilde u_2 + \alpha(x)\tilde w + p_1(x)\tilde w(t,0) \tag{31b}$$

$$\partial_t\tilde u_2 + \gamma_2\partial_x\tilde u_2 = \sigma_{21}\tilde u_1 + \sigma_{22}\tilde u_2 + \alpha(x)\tilde w + p_2(x)\tilde w(t,0) \tag{31c}$$

$$\tilde w(t,1) = \rho_1\tilde u_1(t,1) + \rho_2\tilde u_2(t,1), \tag{31d}$$

$$\tilde u_i(t,0) = 0 \quad \text{for } i=1,2. \tag{31e}$$

Next, we employ a backstepping transformation to prove the exponential stability of the error system (31).

4.1. Backstepping transformation and target error system

We consider the backstepping transformation (Di Meglio et al., 2013)

$$\tilde u_i(t,x) = \tilde\pi_i(t,x) + \int_0^x m_i(x,\xi)\tilde\phi(t,\xi)\,d\xi \quad i=1,2, \tag{32a}$$

$$\tilde w(t,x) = \tilde\phi(t,x) + \int_0^x m_3(x,\xi)\tilde\phi(t,\xi)\,d\xi, \tag{32b}$$

to map (31) into the following target system

$$\partial_t\tilde\pi_1 + \gamma_1\partial_x\tilde\pi_1 = \sigma_{11}\tilde\pi_1 + \sigma_{12}\tilde\pi_2 + \int_0^x g_{11}(x,\xi)\tilde\pi_1(t,\xi)\,d\xi + \int_0^x g_{12}(x,\xi)\tilde\pi_2(t,\xi)\,d\xi, \tag{33a}$$

$$\partial_t\tilde\pi_2 + \gamma_2\partial_x\tilde\pi_2 = \sigma_{21}\tilde\pi_1 + \sigma_{22}\tilde\pi_2 + \int_0^x g_{21}(x,\xi)\tilde\pi_1(t,\xi)\,d\xi + \int_0^x g_{22}(x,\xi)\tilde\pi_2(t,\xi)\,d\xi, \tag{33b}$$

$$\partial_t\tilde\phi - \mu\partial_x\tilde\phi = \theta_1(x)\tilde\pi_1 + \theta_2(x)\tilde\pi_2 + \int_0^x h_1(x,\xi)\tilde\pi_1(t,\xi)\,d\xi + \int_0^x h_2(x,\xi)\tilde\pi_2(t,\xi)\,d\xi, \tag{33c}$$

with the boundary conditions

$$\tilde\pi_i(t,0) = 0, \qquad \tilde\phi(t,1) = \rho_1\tilde\pi_1(t,1) + \rho_2\tilde\pi_2(t,1), \tag{34a}$$

$i = \{1,\ 2\}$. Here, the functions g_{ij} and h_i have to be determined on the triangular domain $\mathbb{T}$. Differentiating the transformations (32) with respect to t and x, and substituting the results into (31) with the help of (33), the following PDEs are derived

$$\gamma_1\partial_x m_1 - \mu\partial_\xi m_1 = \sigma_{11}m_1 + \sigma_{12}m_2 + \alpha(x)m_3, \tag{35a}$$

$$\gamma_2\partial_x m_2 - \mu\partial_\xi m_2 = \sigma_{21}m_1 + \sigma_{22}m_2 + \alpha(x)m_3, \tag{35b}$$
$$\mu\partial_x m_3 + \mu\partial_\xi m_3 = -\theta_1(x)m_1 - \theta_2(x)m_2, \tag{35c}$$
$$m_1(x,x) = \frac{1}{\gamma_1+\mu}\alpha(x), \qquad m_2(x,x) = \frac{1}{\gamma_2+\mu}\alpha(x), \tag{35d}$$
$$m_3(1,\xi) = \rho_1 m_1(1,\xi) + \rho_2 m_2(1,\xi). \tag{35e}$$

The observer gains introduced in (31), are defined by

$$p_i(x) = \mu m_i(x,0) \quad \text{for } i = 1,\ 2,\ 3, \tag{36}$$

and the integral coupling coefficients of the target system (33) are given by

$$h_i(x,\xi) = -\theta(\xi)m_3(x,\xi) - \int_\xi^x m_3(x,s)h_i(s,\xi)\,ds, \tag{37a}$$
$$g_{i,j}(x,\xi) = -\theta_j(\xi)m_i(x,\xi) - \int_\xi^x m_i(x,s)h_j(s,\xi)\,ds, \quad \text{for } \{i,\ j\} = 1,\ 2. \tag{37b}$$

4.2. Inverse transformation

The continuity of the kernel m_3 defined in (32b) guarantees the existence of a unique continuous inverse kernel r_3, which satisfies the following relations

$$\tilde\phi(t,x) = \tilde w(t,x) + \int_0^x r_3(x,\xi)\tilde w(t,\xi)\,d\xi, \tag{38}$$
$$r_3(x,\xi) = -m_3(x,\xi) - \int_\xi^x m_3(x,s)r_3(s,\xi)\,ds \tag{39}$$

defined on $\mathbb{T}$. Substituting (39) into (32a), we obtain

$$\tilde\pi_i(t,x) = \tilde u_i(t,x) + \int_0^x r_i(x,\xi)\tilde w(t,\xi)\,d\xi, \quad i = 1,\ 2 \tag{40}$$
$$r_i(x,\xi) = -\tilde m_i(x,\xi) - \int_\xi^x m_i(x,s)r_3(s,\xi)\,ds.$$

4.3. Exponential convergence of the observer

We first prove exponential stability of the observer target system (33) by the following lemma

Lemma 2. *Under the assumptions $\psi_1^0,\ \psi_2^0,\ \chi^0 \in \mathscr{L}^2([0,1])$ and g_{ij}, $h_i \in \mathscr{C}(\mathbb{T})$, the system (33) with boundary conditions (34) and given initial condition $(\psi_1^0,\ \psi_2^0,\ \chi^0)$ is exponentially stable in the $\mathscr{L}^2$ sense.*

Proof. Consider the following Lyapunov function

$$V_2(t) = \int_0^1 \left[a_2 e^{-\delta_2 x}\left(\frac{\tilde\pi_1^2(t,x)}{\gamma_1} + \frac{\tilde\pi_2^2(t,x)}{\gamma_2}\right) + \frac{e^{\delta_2 x}}{\mu}\tilde\phi^2(t,x)\right]dx, \tag{41}$$

where a_2 and δ_2 are strictly positive parameters to be determined. Differentiating (41) with respect to time along the solution of the target system (33) and integrating by parts, we get

$$\begin{aligned}\dot V_2(t) = &\left[-a_2 e^{-\delta_2 x}(\tilde\pi_1^2(t,x) + \tilde\pi_2^2(t,x)) + e^{\delta_2 x}\tilde\phi^2(t,x)\right]_0^1 - \delta_2\int_0^1 e^{\delta_2 x}\tilde\phi^2(t,x)\,dx\\ &+ 2\int_0^1 a_2 e^{-\delta_2 x}\Pi^T(t,x)\mathbf{\Gamma}_{inv}\boldsymbol{\sigma}\,\Pi(t,x)dx\\ &- \delta_2\int_0^1 a_2 e^{-\delta_2 x}\Pi^T(t,x)\,\Pi(t,x)\,dx\\ &+ 2\int_0^1\int_0^x a_2 e^{-\delta_2 x}\Pi^T(t,x)\mathbf{\Gamma}_{inv}\mathbf{G}(x,\xi)\,\Pi(t,\xi)d\xi\,dx\\ &+ 2\int_0^1 \frac{e^{\delta_2 x}}{\mu}\tilde\phi(t,x)\boldsymbol{\theta}(x)\Pi(t,x)dx\\ &+ 2\int_0^1 \frac{e^{\delta_2 x}}{\mu}\tilde\phi(t,x)\int_0^x \boldsymbol{h}(x,\xi)\Pi(t,\xi)\,d\xi\,dx,\end{aligned}$$

where the vector Π, $\boldsymbol{\theta}$, $\boldsymbol{h}$ and the matrix $\boldsymbol{G}$ are given by

$$\Pi(t,x) = \begin{pmatrix}\tilde\pi_1(t,x)\\ \tilde\pi_2(t,x)\end{pmatrix}, \qquad \boldsymbol{G}(x,\xi) = \begin{pmatrix}g_{11}(x,\xi) & g_{12}(x,\xi)\\ g_{21}(x,\xi) & g_{22}(x,\xi)\end{pmatrix},$$
$$\boldsymbol{\theta}(x) = \begin{pmatrix}\theta_1(x) & \theta_2(x)\end{pmatrix}, \qquad \boldsymbol{h}(x,\xi) = \begin{pmatrix}h_1(x,\xi) & h_2(x,\xi)\end{pmatrix}.$$

Assuming the existence of a constant $\tilde M > 0$ such that

$$\|\boldsymbol{G}(x,\xi)\|,\ \|\boldsymbol{\theta}(x)\|,\ \|\boldsymbol{h}(x,\xi)\| \le \tilde M, \quad \forall x \in [0,1], \xi \in [0,x],$$

we deduce the following estimate

$$\begin{aligned}\dot V_2(t) \le &-e^{-\delta_2}\left[\left(a_2 - 2\rho_1^2 e^{2\delta_2}\right)\tilde\pi_1^2(t,1) + \left(a_2 - 2\rho_2^2 e^{2\delta_2}\right)\tilde\pi_2^2(t,1)\right]\\ &- \int_0^1 e^{\delta_2 x}\left(\delta_2 - \frac{1+x}{\mu}\right)\tilde\phi^2(t,x)\,dx\\ &- \int_0^1 \Pi^T(t,x)e^{-\delta_2 x}\tilde P(x)\,\Pi(t,x)dx,\end{aligned} \tag{42}$$

where

$$\tilde P(x) = a_2\left(\delta_2 - \frac{(2+x+1/\delta_2)\tilde M}{\varepsilon}\right) + e^{2\delta_2 x}\left(\frac{1}{\delta_2} - 1\right)\frac{\tilde M^2}{\mu} - \frac{\tilde M^2}{\delta_2\mu}e^{\delta_2(1+x)}. \tag{43}$$

We choose $\delta_2 > \frac{1+x}{\mu}$ and

$$a_2 > \max\left\{2\rho_1^2 e^{2\delta_2}, 2\rho_2^2 e^{2\delta_2}, -\frac{e^{2\delta_2 x}\left(\frac{1}{\delta_2} - 1\right)\frac{\tilde M^2}{\mu} - \frac{\tilde M^2}{\delta_2\mu}e^{\delta_2(1+x)}}{\delta_2 - \frac{(2+x+1/\delta_2)\tilde M}{\varepsilon}}\right\} \tag{44}$$

to ensure the positiveness of the matrix $P(x)$, $x \in [0,1]$. Hence, $\dot V_2 < 0$, which guarantees exponential stability of the target error system. From the continuity and invertibility of the backstepping transformation (32), exponential convergence of the designed observer is obtained and the following theorem holds.

Theorem 2. *Under the assumptions that the initial data are in $\left(\mathscr{L}^2([0,1])\right)^3$, the observer system (29a)–(29c) (with the coefficient functions $p_i(x)$, $i = \overline{1,3}$ determined by (35)–(36)) and with the boundary conditions (29d)–(29e) exponentially converge to the system (9) in the $\mathscr{L}^2$ sense.*

5. Output feedback control

Combining the controller (20), which requires a full state measurement, and the observer (29), which reconstructs the distributed state based on an output measurement $w(t,0)$, we design an observer-based output feedback controller.

Theorem 3. *Consider the* $(u_1,\ u_2,\ w)^T$*-system* (9) *together with the* $(\hat{u}_1,\ \hat{u}_2,\ \hat{w})^T$*-observer* (29)*. For a given initial condition* $(u_1^0,\ u_2^0,\ w^0,\ \hat{u}_1^0,\ \hat{u}_2^0,\ \hat{w}^0)^T \in \left(\mathscr{L}^2([0,\ 1])\right)^6$ *and the control law*

$$U(t) = -\rho_1 u_1(t,1) - \rho_2 u_2(t,1) + \int_0^1 \Big[k_1(1,\xi)\hat{u}_1(x,\xi) + k_2(1,\xi)\hat{u}_2(x,\xi) + k_3(1,\xi)\hat{w}(1,\xi)\Big]\,d\xi, \tag{45}$$

where k_1*,* k_2 *and* k_3 *satisfy* (13)*, the* $(u_1,\ u_2,\ w,\ \hat{u}_1,\ \hat{u}_2,\ \hat{w})^T$*-system is exponentially stable in the sense of the* $\mathscr{L}^2$*-norm.*

Proof. From the definition of the error variable vector (30), the combined closed-loop $(u_1,\ u_2,\ w,\ \hat{u}_1,\ \hat{u}_2,\ \hat{w})^T$-system is equivalent to the $(\hat{u}_1,\ \hat{u}_2,\ \hat{w},\ \tilde{u}_1,\ \tilde{u}_2,\ \tilde{w})^T$-system. In comparison to the backstepping transformation (10) and (11), the invertible transformation

$$\hat{\psi}_i(t,x) = \hat{u}_i(t,x) \quad \text{for } i = 1,\ 2 \tag{46}$$

$$\hat{\chi}(t,x) = \hat{w}(t,x) - \int_0^x k_1(x,\xi)\hat{u}_1(t,\xi)\,d\xi - \int_0^x k_2(x,\xi)\hat{u}_2(t,\xi)\,d\xi - \int_0^x k_3(x,\xi)\hat{w}(t,\xi)\,d\xi \tag{47}$$

and (32) maps the system (29) into a $(\hat{\psi}_1,\ \hat{\psi}_2,\ \hat{\chi},\ \tilde{\pi}_1,\ \tilde{\pi}_2,\ \tilde{\phi})^T$-system, of which the exponential stability can be proved with the help of the following Lyapunov function

$$V(t) = \int_0^1 a_1 e^{-\delta_1 x}\left(\frac{\hat{\psi}_1^2(t,x)}{\gamma_1} + \frac{\hat{\psi}_2^2(t,x)}{\gamma_2}\right)dx + \int_0^1 \frac{1+x}{\mu}\hat{\chi}^2(t,x)dx + b\int_0^1 \frac{e^{\delta_2 x}}{\mu}\tilde{\phi}^2(t,x)dx + b\int_0^1 a_2 e^{-\delta_2 x}\left(\frac{\tilde{\pi}_1^2(t,x)}{\gamma_1} + \frac{\tilde{\pi}_2^2(t,x)}{\gamma_2}\right)dx. \tag{48}$$

Exponential stability of the $(u_1,\ u_2,\ w,\ \hat{u}_1,\ \hat{u}_2,\ \hat{w})^T$-system is thus proved.

6. Numerical simulations

This section is devoted to numerical simulations of the system (8) using respectively the controllers $U(t)$ defined in (20) and (47). Our goal is to demonstrate the performance of the suggested controllers (20) and (47) in stabilizing system (8) around the zero equilibrium. We employ an accurate finite volume scheme (a modified Roe scheme) to advance in time and space the hyperbolic evolutionary system (8). Elsewhere, for the implementation of the control law (47), the computation of the kernel PDE's system (13) on $\mathbb{T}$ is achieved using a finite element setup. The initial bottom topography is defined as

$$B(0,x) = 0.4\Big(1 + 0.25\exp\Big(-\frac{(x-0.5)^2}{0.003}\Big)\Big),$$

with a Gaussian distribution centered at the middle of the domain. The initial water level and its velocity field are computed as $H(0,x) = 2.5 - B(0,x)$ and $H(0,x)V(0,x) = 10\sin(\pi x)$, respectively.

Using the initial conditions of system (1), namely, $H(0,x)$, $V(0,x)$ and $B(0,x)$, the initial data of the characteristic variables v, u_1 and u_2 are computed from (4).

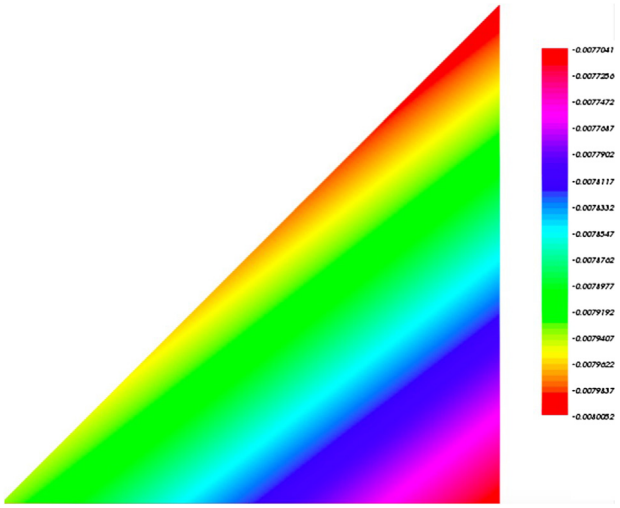

Fig. 4. Numerical solution of the kernel k_1 on $\mathbb{T}$.

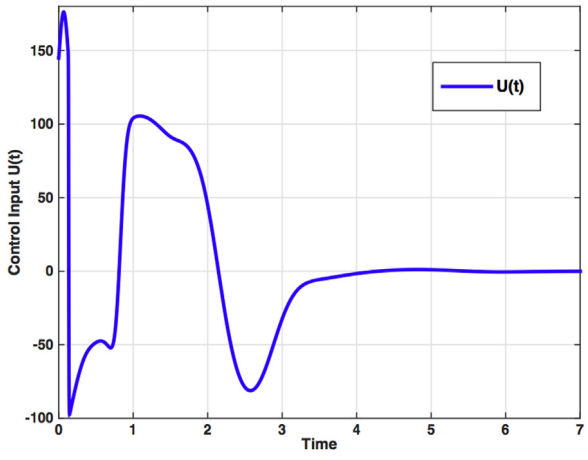

Fig. 5. Evolution of the control $U(t)$.

6.1. State feedback under subcritical flow regime ($Fr < 1$)

For a subcritical flow regime, we consider the set point $(H^*,\ V^*,\ B^*)$ defined in Table 1 (see Appendix), which leads to the characteristic speeds $\lambda_1 = -1.42$, $\lambda_2 = 0.76$ and $\lambda_3 = 7.42$, and the Froude number $Fr = 0.6$. The coefficients α_i, θ_i and the matrix $\boldsymbol{\sigma}$ are computed with the help of the characteristics speeds λ_i. In order to implement the state feedback controller (20), the values of the kernels k_1, k_2 and k_3 at $x = 1$ are derived from the numerical computation of (13) as it is shown in Fig. 4. Despite the large initial amplitudes, the control input $U(t)$ (see Fig. 5) and the output measurement $y(t)$ (see Fig. 6) converge to the zero equilibrium after $t \geq 4$ s.

Fig. 7 shows the convergence of the norm of the characteristics to zero. Therefore system (9) converges to the zero equilibrium and thereby, the linearized model (2) converges to $(H^*,\ V^*,\ B^*)$.

6.2. Output feedback under supercritical flow ($Fr > 1$)

For supercritical flow regime, the parameters of the physical model are listed in Table 2 (see Appendix). The set point $(H^*,\ V^*,\ B^*)$ leads to the characteristic velocities $\lambda_1 = 1.87$, $\lambda_2 = -0.74$ and $\lambda_3 = 8.13$ and the Froude number $Fr = 1.6$. The dynamics of the closed-loop system (8), together with the output feedback control law (47), is simulated. In order to implement the feedback control law (47), the kernel PDEs (13) and (35) are solved

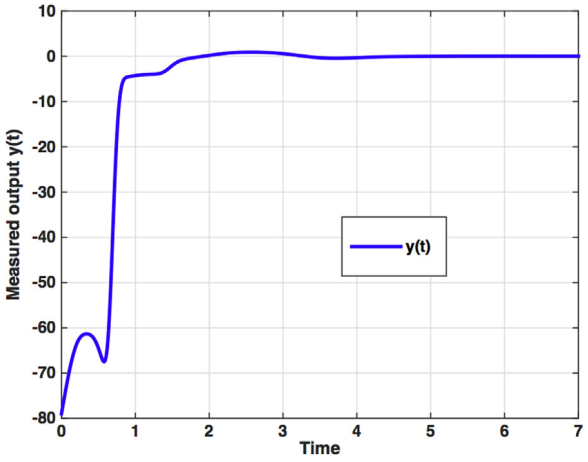

Fig. 6. Evolution of the measured output $y(t)$.

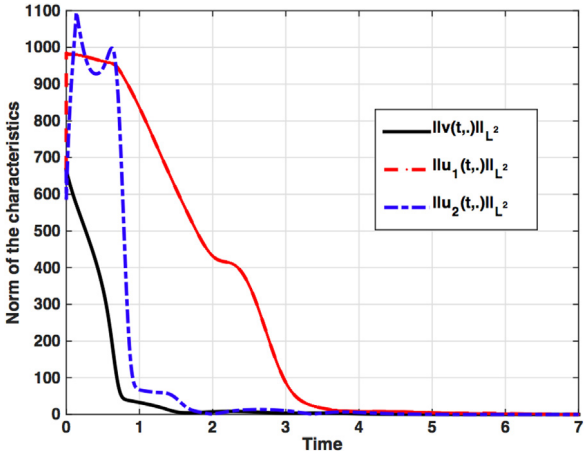

Fig. 7. Evolution of the norm of the characteristic solution.

numerically. The kernel gain $p_i(x)$ defined in (36) are depicted in Fig. 8. The computation of the control law (47) also requires the solution of the system (33)–(34), which is solved numerically on time and space using a finite element setup. Fig. 9 shows the evolution in time of the control input $U(t)$ at downstream, and the output measurement $y(t)$ at upstream. Clearly, the amplitudes of

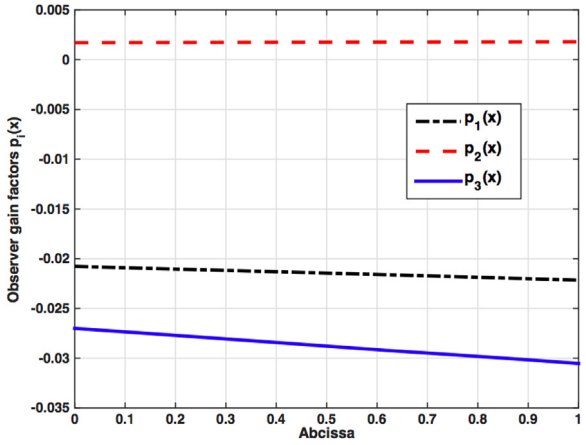

Fig. 8. Computed observer gains $p_i(x)$.

$U(t)$ and $y(t)$ decrease in time and vanishes for $t \geq 4$ s as shown in Fig. 9(a) and (b), respectively.

The dynamics of the $\mathscr{L}^2$-norm are directly related to the magnitude of the propagation speeds λ_i (see Fig. 10). Under this supercritical flow regime, it is remarkable that the backstepping output feedback control law (Fig. 10(a)) achieves exponential stability compared to the approach in Diagne et al. (2012) (Fig. 10(b)), which leads to an unstable dynamics. Fig. 11 describes the space and time dynamics of the plant, and is consistent with the numerical results presented above. As time increases, it can be noticed that the perturbation in the overall system decreases and vanishes later.

7. Concluding remarks

This paper considers the stabilization of a linearized Saint-Venant–Exner model. A backstepping state feedback controller is first designed for the stabilization of the water level and the bathymetry at a desired equilibrium set. Using an exponentially convergent Luenberger observer, we design a backstepping output feedback controller with the measurements at upstream, which also achieves the exponential stability of the linearized SVE model, for both subcritical and supercritical flow regime. Although the backstepping approach offers a more complicated design than the method developed in Diagne et al. (2012), it enables exponential stabilization of the SVE system without any restriction on the system and the nature of the flow. Also, with the backstepping

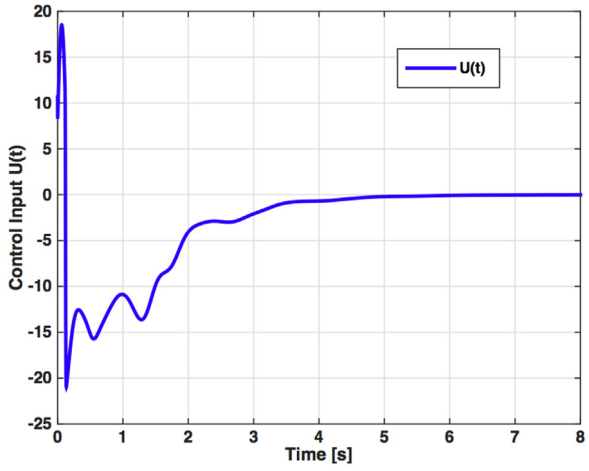

(a) Output control law.

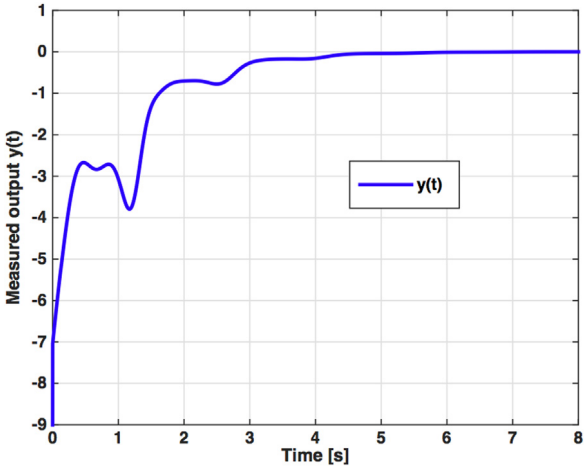

(b) Measured output.

Fig. 9. Evolution of the control law and the measured output.

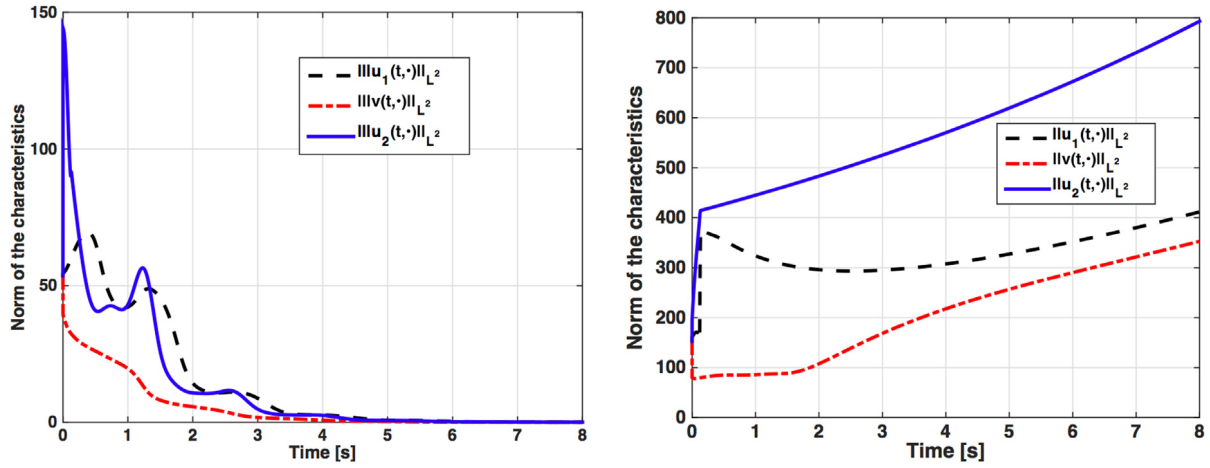

(a) Backstepping design.

(b) Lyapunov design (Diagne et al., 2012).

Fig. 10. Evolution of the norms of the characteristic solutions.

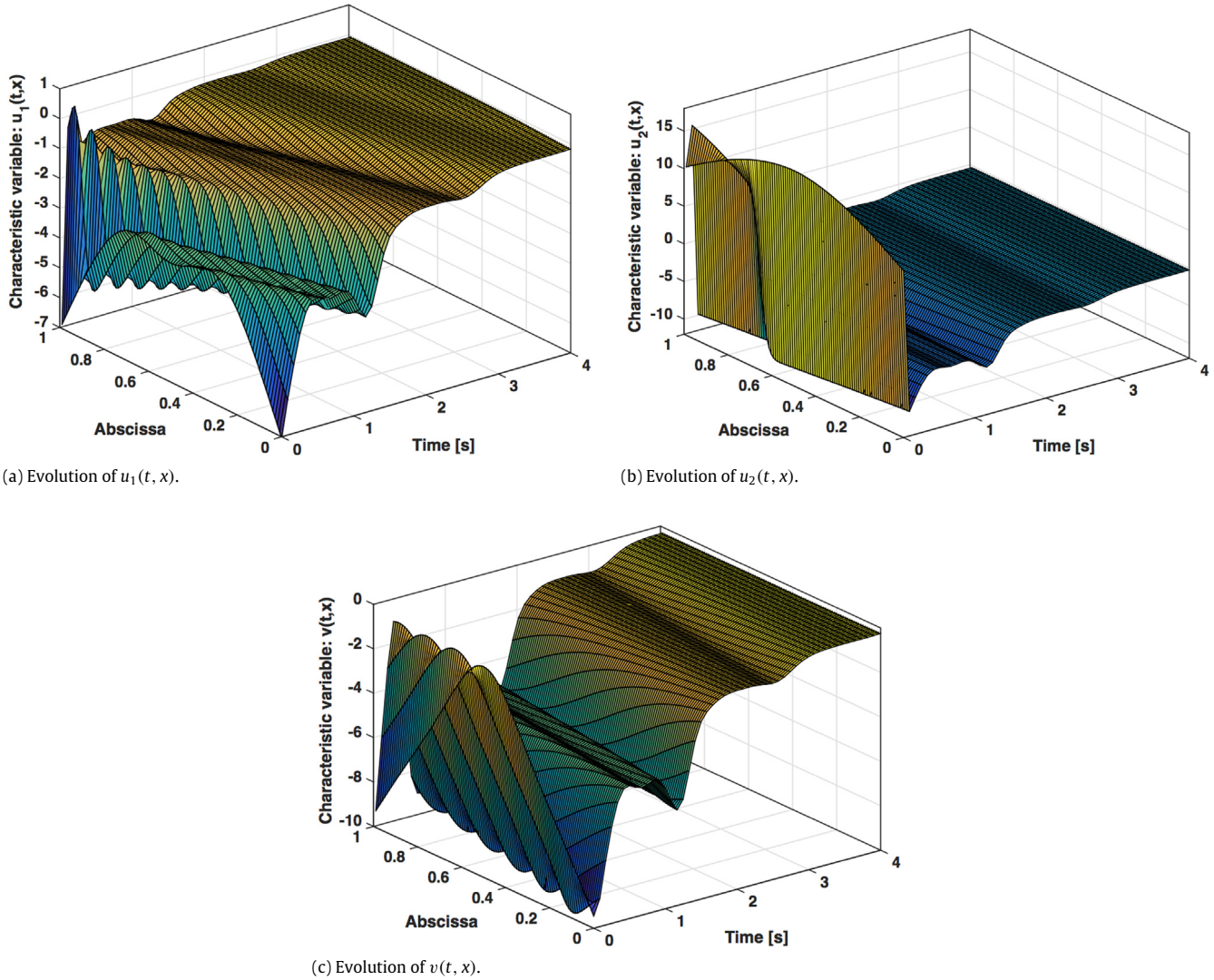

(a) Evolution of $u_1(t,x)$.

(b) Evolution of $u_2(t,x)$.

(c) Evolution of $v(t,x)$.

Fig. 11. Behavior in time and space of the distributed states.

controller, only a single boundary control is needed compared to Diagne et al. (2012). One should mention that only the free water surface level is measured at two boundaries in the feedback control law introduced in Diagne et al. (2012). Our future works are to consider disturbance rejection issues for this application (Tang, Guo, & Krstic, 2014; Tang & Krstic, 2014), as well as the adaptive estimation and control problems with unknown boundary parameters (Anfinsen, Diagne, Aamo, & Krstic, 2016; He,

Table 1
Parameters of the subcritical flow regime.

CFL	A	ρ_1	ρ_2	H^*	U^*	B^*
0.95	0.008	1.5	1.5	2	3	0.4

Table 2
Parameters of supercritical flow regime.

CFL	A_g	ρ_1	ρ_2	H^*	U^*	B^*
0.9	0.003	1	1.5	1	5	0.4

Ge, & Zhang, 2011; Zhang, Xu, & Zhang, 2014) and constrained output due to the outflow gate operation (He & Ge, 2015).

Appendix

$T = 8$, $\Delta x = 0.01$, $p = 0.002$, $C_f = 0.002$, $\rho_2 = 1.5$, $q_1 = 1$, $q_2 = 1.2$.

References

Anfinsen, H., Diagne, M., Aamo, O. M., & Krstic, M. (2016). An adaptive observer design for n+1 coupled linear hyperbolic PDEs based on swapping. *IEEE Transactions on Automatic Control*, http://dx.doi.org/10.1109/TAC.2016.2530624.

Balogun, O. S., Hubbard, M., & DeVries, J. J. (1988). Automatic control of canal flow using linear quadratic regulator theory. *Journal of Hydraulic Engineering*, *114*(1), 75–102.

Coron, J. M., Vazquez, R., Krstic, M., & Bastin, G. (2013). Local exponential H^2 stabilization of a 2×2 quasilinear hyperbolic system using backstepping. *SIAM Journal on Control and Optimization*, *51*(3), 2005–2035.

Daly, E., & Porporato, A. (2005). Some self-similar solutions in river morphodynamics. *Water Resources Research*, *41*(12).

Di Meglio, F., Vazquez, R., & Krstic, M. (2013). Stabilization of a system of coupled first-order hyperbolic linear PDEs with a single boundary input. *IEEE Transactions on Automatic Control*, *58*(12), 3097–3111.

Diagne, A., Bastin, G., & Coron, J. M. (2012). Lyapunov exponential stability of 1-d linear hyperbolic systems of balance laws. *Automatica*, (1), 109–114.

Diagne, M., Santos Martins, V. Dos, & Rodrigues, M. (2010). Une approche multi-modèles des équations de saint-venant: une analyse de la stabilité par techniques lmi. In *Proceedings of sixième conférence internationale francophone d'automatique, CIFA, Nancy, France*.

Diagne, A., & Sène, A. (2013). Control of shallow water and sediment continuity coupled system. *Mathematics of Control, Signal, and Systems (MCSS)*, 387–406.

He, W., & Ge, S. S. (2015). Vibration control of a flexible beam with output constraint. *IEEE Transactions on Industrial Electronics*, *62*(8), 5023–5030.

He, W., Ge, S. S., & Zhang, S. (2011). Adaptive boundary control of a flexible marine installation system. *Automatica*, *47*(12), 2728–2734.

Hudson, J., & Sweby, P. K. (2003). Formulations for numerically approximating hyperbolic systems governing sediment transport. *Journal of Scientific Computing*, *19*, 225–252.

Krstic, M., & Smyshlyaev, A. (2008). *Boundary control of PDEs: A course on backstepping designs. Vol. 16*. SIAM.

Lanzoni, S., Siviglia, A., Frascati, A., & Seminara, G. (2006). Long waves in erodible channels and morphodynamic influence. *Water Resources Research*, *42*(6).

Litrico, X., & Fromion, V. (2006). H^∞ control of an irrigation canal pool with a mixed control politics. *IEEE Transactions on Control Systems Technology*, *14*(1), 99–111.

Malaterre, P. O., Rogers, D. C., & Schuurmans, J. (1998). Classification of canal control algorithms. *Journal of Irrigation and Drainage Engineering*, *124*(1), 3–10.

Pognant-Gros, P., Fromion, V., & Baume, J.P. (2001). Canal controller design: a multivariable approach using h infini. In *Proceedings of the European control conference, Portugal* (pp. 3398–3403).

Prieur, C., & de Halleux, J. (2004). Stabilization of a 1-d tank containing a fluid modeled by the shallow water equations. *Systems & Control Letters*, *52*(3–4), 167–178.

Santos Martins, V. Dos, Rodrigues, M., & Diagne, M. (2008). A multi-models approach of saint-venant's equations: A stability study by LMI. *International Journal of Applied Mathematics and Computer Science*, *22*(3), 539–550.

Tang, S.-X., Guo, B.-Z., & Krstic, M. (2014). Active disturbance rejection control for 2×2 hyperbolic systems with input disturbance. In *IFAC world congress* (pp. 1027–1032).

Tang, S.-X., & Krstic, M. (2014). Sliding mode control to the stabilization of a linear 2×2 hyperbolic system with boundary input disturbance. In *American control conference (ACC)* (pp. 1027–1032). IEEE.

Tang, Y., Prieur, C., & Girard, A. (2014). Boundary control synthesis for hyperbolic systems: a singular perturbation approach. In *IEEE conference on decision and control, Los Angeles, California, USA*.

Xu, C.Z., & Sallet, G. (1999). Proportional and integral regulation of irrigation canal systems governed by the saint-venant equation. In *In Proceedings of the 14th world congress IFAC, Beijing* (pp. 147–152).

Zhang, Z., Xu, S., & Zhang, B. (2014). Asymptotic tracking control of uncertain nonlinear systems with unknown actuator nonlinearity. *IEEE Transactions on Automatic Control*, *59*(5), 1336–1341.

Ababacar Diagne is a post-doctoral researcher at the Department of Scientific Computing, Uppsala University. He received a Graduate Degree in Applied Mathematics and Computer Sciences from the Gaston Berger University of Saint-Louis (Sénégal) in 2007 and a Ph.D. in Applied Mathematics with specialization in numerical analysis jointly at Gaston Berger University of Saint-Louis and Royal Institute of Technology (Sweden) in 2012. His research interests include finite element methods for flow problems, parallel implementations in modern scientific software and control of hyperbolic systems with applications in environmental systems.

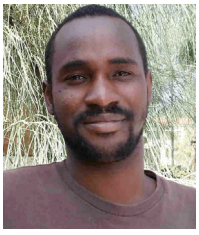

Mamadou Diagne received his Ph.D. degree in 2013 at Université Claude Bernard Lyon I in France. He has been a doctoral fellow at Laboratoire d'Automatique et du Génie des Procédés, in Lyon (France). From 2013 to 2015, he was a postdoctoral fellow at the University of California San Diego and is currently a postdoctoral fellow at the University of Michigan Ann Arbor. His research interests concern the modeling and the control of heat and mass transport processes described by partial differential equations and delay systems.

Shuxia Tang received her Ph.D. in Mechanical Engineering in 2016 from the Department of Mechanical & Aerospace Engineering, University of California, San Diego, USA. Her main research interests are stability analysis and control design of distributed parameter systems. Moreover, lithium-ion battery applications and multi-agent cooperative control also fall into her research interests.

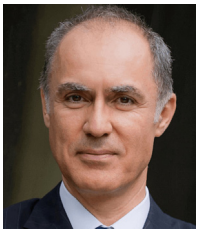

Miroslav Krstic holds the Alspach endowed chair and is the founding director of the Cymer Center for Control Systems and Dynamics at UC San Diego. He also serves as Associate Vice Chancellor for Research at UCSD. As a graduate student, Krstic won the UC Santa Barbara best dissertation award and student best paper awards at CDC and ACC. Krstic is Fellow of IEEE, IFAC, ASME, SIAM, and IET (UK), Associate Fellow of AIAA, and foreign member of the Academy of Engineering of Serbia. He has received the PECASE, NSF Career, and ONR Young Investigator awards, the Axelby and Schuck paper prizes, the Chestnut textbook prize, the ASME Nyquist Lecture Prize, and the first UCSD Research Award given to an engineer. Krstic has also been awarded the Springer Visiting Professorship at UC Berkeley, the Distinguished Visiting Fellowship of the Royal Academy of Engineering, the Invitation Fellowship of the Japan Society for the Promotion of Science, and the Honorary Professorships from the Northeastern University (Shenyang), Chongqing University, and Donghua University, China. He serves as Senior Editor in IEEE Transactions on Automatic Control and Automatica, as editor of two Springer book series, and has served as Vice President for Technical Activities of the IEEE Control Systems Society and as chair of the IEEE CSS Fellow Committee. Krstic has coauthored eleven books on adaptive, nonlinear, and stochastic control, extremum seeking, control of PDE systems including turbulent flows, and control of delay systems.